

February 15, 1984

## Electronic structure of copper-rich copper-palladium alloys

R. S. Rao

*Tampere University of Technology*

A. Bansil

*Northeastern University*

H. Asonen

*Tampere University of Technology*

M. Pessa

*Tampere University of Technology*

---

### Recommended Citation

Rao, R. S.; Bansil, A.; Asonen, H.; and Pessa, M., "Electronic structure of copper-rich copper-palladium alloys" (1984). *Physics Faculty Publications*. Paper 374.

## Electronic structure of copper-rich copper-palladium alloys

R. S. Rao

*Physics Department, Tampere University of Technology, SF-33101 Tampere 10, Finland  
and Physics Department, Northeastern University, Boston, Massachusetts 02115*

A. Bansil

*Physics Department, Northeastern University, Boston, Massachusetts 02115*

H. Asonen and M. Pessa

*Physics Department, Tampere University of Technology, SF-33101 Tampere 10, Finland*

(Received 22 August 1983)

In considering the electronic structure of (Cu-rich) CuPd alloys, we present computations of complex-energy bands and average densities of states together with the angle-resolved photoemission spectra from the (100), (111), and (110) surfaces of Cu<sub>95</sub>Pd<sub>5</sub> and Cu<sub>85</sub>Pd<sub>15</sub> single crystals. The impurity spectrum in CuPd is found to be dominated by two quite-well-separated Pd-derived impurity bands and differs sharply from the case of CuNi or AgPd systems, where only a single Ni- or Pd-related impurity structure appears in the alloy. Extensive comparisons between the theory and experiment are carried out with regard to the positions and halfwidths of the Pd-induced impurity structures, the level shifts and disorder smearings of the Cu-derived bands, and the shifts in the binding energies of the Cu 2*p* and Pd 3*d* core levels. A remarkably good agreement is found to exist in all cases. The (111) Shockley state is observed to lie at a binding energy of 0.2 eV (with respect to the Fermi energy) in Cu<sub>95</sub>Pd<sub>5</sub> and to possess an increased full width at half maximum (compared to Cu) of 60 meV. This state moves just above the Fermi energy in Cu<sub>85</sub>Pd<sub>15</sub>. These effects can also be understood in terms of the changes in the bulk electronic spectrum of Cu upon alloying with Pd.

## I. INTRODUCTION

The electronic structure of disordered alloys has been the subject of extensive investigations during the last decade, culminating in the development of a band theory of alloys within the framework of the Korringa-Kohn-Rostoker coherent-potential approximation (KKR-CPA) and its simpler version, the average-*t*-matrix approximation (ATA).<sup>1-3</sup> This approach involves the application of the ideas of ATA and CPA, developed earlier in connection with the simple one- and two-band tight-binding-model Hamiltonians, to the muffin-tin Hamiltonian, which is well known as providing a realistic representation of the crystal potentials in perfect metals and presumably also in close-packed disordered materials. It is clear that the KKR-CPA gives a good description of at least the average properties of the medium. On the experimental side, state-of-the-art advances are making it possible to test theoretical predictions at an increasingly sophisticated microscopic level. A note may be made here of progress in the areas of angle-resolved photoemission spectroscopy (ARPES),<sup>4</sup> two-dimensional angular correlation of annihilation radiation,<sup>5</sup> and the differential (composition modulation) optical reflectivity studies.<sup>6</sup> In recent papers we have discussed at some length the electronic spectra of CuAl and CuGe solid solutions, using the ARPES spectra from low-index faces of alloy single crystals together with the KKR-CPA computations.<sup>7,8</sup> Here we consider the Cu-rich CuPd system which constitutes an example of a transition-metal impurity in Cu. In comparison to the

earlier angle-integrated photoemission experiments,<sup>9-11</sup> the present angle-resolved measurements provide a substantially more detailed picture of the electronic spectrum.

An outline of this paper and its principal conclusions is as follows: Section II discusses the underlying theoretical spectrum of CuPd alloys. The Cu and Pd muffin-tin potentials used in this work are described and the KKR-CPA computations in Cu<sub>95</sub>Pd<sub>5</sub> and Cu<sub>85</sub>Pd<sub>15</sub> are presented. The impurity spectrum is found to be dominated by two quite-well-separated Pd-derived impurity bands and thus differs sharply from the case of CuNi or AgPd, where only a single Ni- or Pd-related impurity structure appears in the alloy.<sup>10-14</sup> This phenomenon physically has its origin in the large-crystal-field splitting associated with the Pd muffin-tin potential in the alloy and also in the particular circumstance that the Cu *d* band lies roughly in the middle of the substantially broader Pd *d* band. The Pd *d* states then tend to get excluded from the middle region and give rise to a two-peaked structure in the density of states on the Pd site. To gain further insight into the preceding effects, we also present and discuss a number of additional KKR-CPA computations involving shifts of the Pd *d* bands to higher as well as to lower energies from their correct position with respect to the Cu *d* bands.

Section III presents He I (21.22 eV) and Ni I (16.85 eV) angle-resolved normal-emission spectra from the (100), (111), and (110) faces of Cu, Cu<sub>95</sub>Pd<sub>5</sub>, Cu<sub>85</sub>Pd<sub>15</sub>, and Pd single crystals. A limited number of off-normal-emission spectra were also investigated. A remarkably wide range of agreement is found to exist between the ARPES mea-

surements and the theoretical picture developed in Sec. II. In this connection we consider the positions and halfwidths of the Pd-induced impurity structures and also the level shifts and disorder smearings of the Cu bands (which continue to be clearly identifiable) in various parts of the Brillouin zone for both the 5- and 15-at. % Pd alloy. The Fermi-surface dimensions of Cu-rich CuPd alloys decrease essentially uniformly and in accord with the predictions of a Cu-based rigid-band model, assuming effective valences of 0 and 1 for Pd and Cu, respectively. The calculated shifts in the positions of the Cu  $2p$  and the Pd  $3d$  core levels are in good accord, in sign and magnitude, with the electron spectroscopy for chemical analysis (ESCA) results of Martensson *et al.*<sup>9</sup> Finally, concerning the intrinsic surface states, we were able to locate the (111) Shockley state clearly in Cu<sub>95</sub>Pd<sub>5</sub> at a 0.2 eV lower binding energy (compared to Cu). In Cu<sub>85</sub>Pd<sub>15</sub>, we deduce from the spectra that this state has moved just above the Fermi energy. (The Tamm-type surface states are not expected to be observable due to the presence of strong Pd emission in their energy range.) We interpret the level shift and smearing of the (111) Shockley state in terms of the changes in the bulk bands of Cu upon alloying and, here again, find good accord with the measurements.

## II. THEORETICAL ELECTRONIC SPECTRUM

The theoretical techniques used in the present KKR-CPA calculations have been discussed at length elsewhere. (See Refs. 12 and 2.) Mattheiss's prescription of overlapping the charge densities was employed to generate the constituent muffin-tin potentials on a composition dependent fcc lattice with the lattice constant of the alloy. Herman-Skillman wave functions corresponding to atomic configurations of  $3d^{10}4s^1$  and  $4d^{10}5s^0$  for Cu and Pd, respectively, were used. The Cu muffin-tin potential is essentially the same as that we have used in other Cu-based systems, except that the Cu  $d$  bands were moved to a 0.15 eV lower energy in order to gain good absolute agreement with the measured Cu  $d$  bands. The Pd potential for the perfect Pd fcc lattice yielded good agreement with the published Pd-band structures.<sup>15</sup> However, the Pd potential generated on the alloy lattice constant leads to unphysical results and was therefore rigidly moved by 0.18 Ry to a lower energy with respect to the Cu potential. This is the only semiempirical adjustment which we have invoked for Pd. However, as the discussion in Sec. III will show, our calculations possess a wide range of agreement with the measurements for both the 5- and 15-at. %

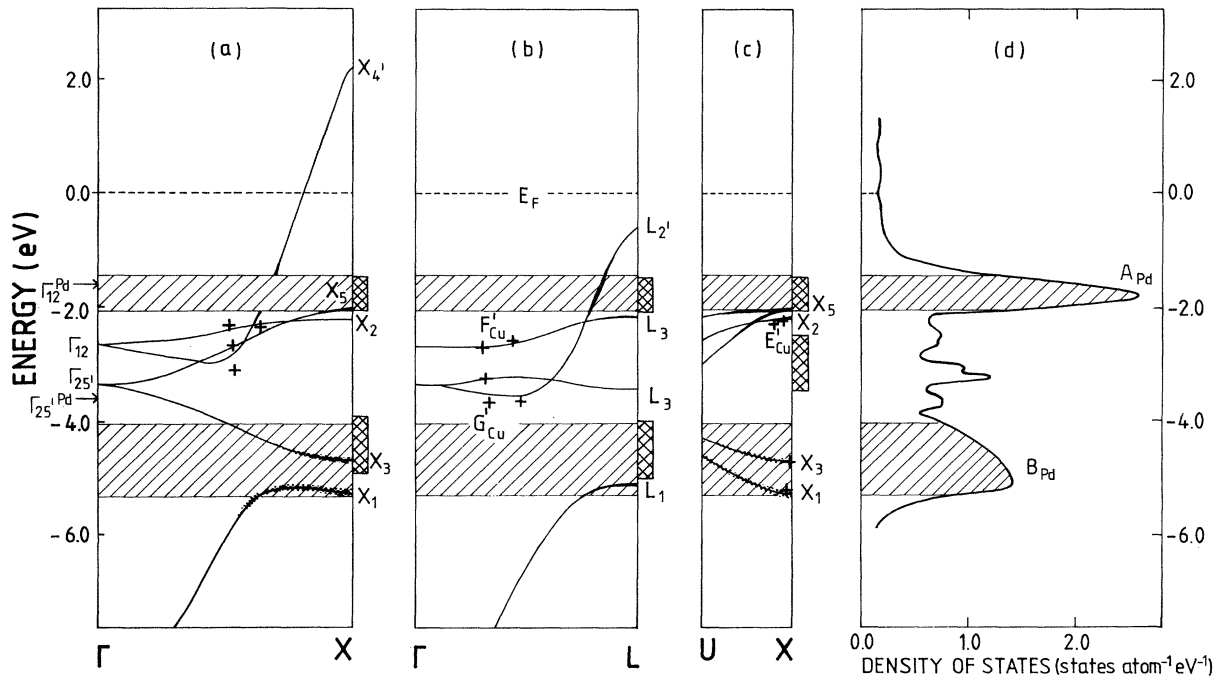


FIG. 1. Electronic spectrum of Cu<sub>95</sub>Pd<sub>5</sub> using the KKR-CPA is compared with the corresponding ARPES results. Complex-energy bands along the  $\Gamma$ - $X$ ,  $\Gamma$ - $L$ , and  $U$ - $X$  symmetry directions are plotted in (a)-(c), while (d) gives the density of states on a Pd site normalized to five states per atom. Vertical length of the shading around the bands equals 2 times the imaginary part of complex energies. The Pd-related bands are generally smeared heavily due to disorder and are not shown (Ref. 17); the bands  $A_{Pd}$  and  $B_{Pd}$  are indicated as hatched regions of full width at half maximum of the associated peaks in (d). The uppermost valence band is shown with a break along the  $\Gamma$ - $X$  direction in (a) because this band hybridizes strongly with the Pd-derived impurity band as it crosses the latter (see text for a discussion). Crosses give the  $E(\vec{k})$  values for a number of Cu-derived  $d$  bands and are obtained by the triangular method from the experimental spectra. The labels  $E_{Cu}$ ,  $F_{Cu}$ , and  $G_{Cu}$  refer to points corresponding to specific spectral features in Figs. 6-8 below. Cross-hatched regions on the right side of panels (a)-(c) give the location and full width at half maximum of the Pd-derived structures in the ARPES spectra. The energies of the  $e_g(\Gamma_{12})$  and  $t_{2g}(\Gamma_{25'})$  levels for the Cu and Pd muffin-tin potentials, used in the alloy computations, are marked on the left-hand side of the figure.

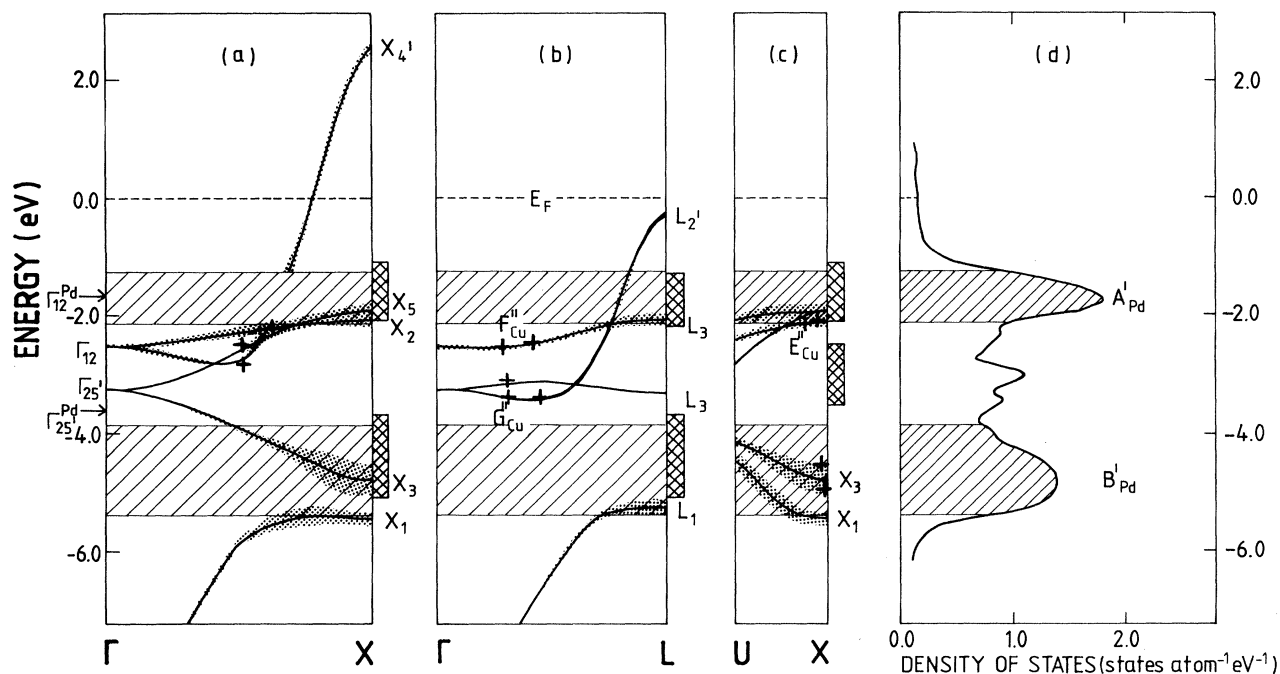


FIG. 2. Same as in Fig. 1, except obvious minor differences in the notation and the fact that this figure refers to  $\text{Cu}_{85}\text{Pd}_{15}$ .

Pd alloys. Two further points are noteworthy in this regard: (i) By computing the absolute positions of the Pd  $3d$  and Cu  $2p$  core levels with respect to the Fermi energy in  $\text{Cu}_{85}\text{Pd}_{15}$  and in the pure Pd and Cu crystals, we obtain an *increased* binding energy of the Pd  $3d$  core levels of 0.7 eV and a *decreased* binding energy of 0.1 eV for the Cu  $2p$

core level. These values are in excellent accord with the corresponding measured values of 0.8 and 0.1 eV, in sign and magnitude, obtained by Martensson *et al.* via ESCA.<sup>9</sup> (ii) Measurements of the electronic structure of Pd overlayers grown epitaxially on the Cu(111) substrate,<sup>16</sup> with increasing Pd coverage, show that the Pd  $d$  bands indeed

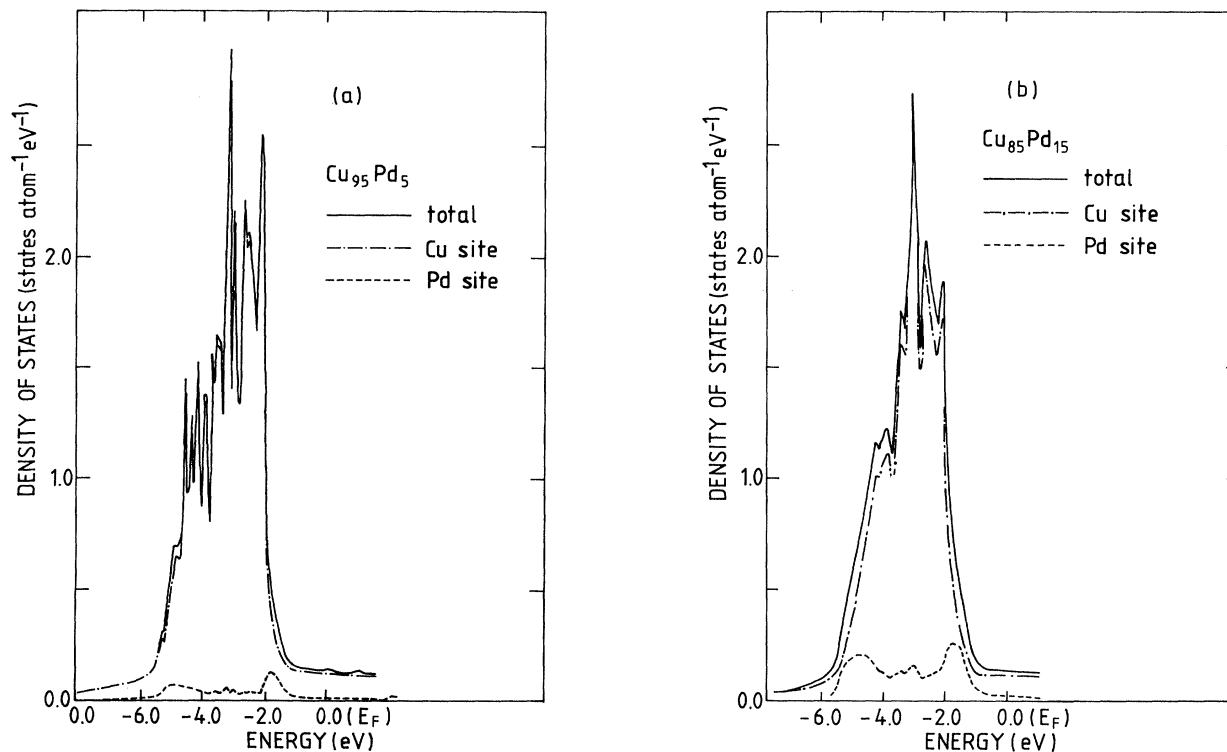


FIG. 3. Average density of states in  $\text{Cu}_{95}\text{Pd}_5$  and  $\text{Cu}_{85}\text{Pd}_{15}$ . The components of the total density associated with the Cu and Pd sites are also shown.

appear well above the Cu  $d$ -band complex, just about where our unadjusted Pd potential places them. It is clear then that the aforementioned adjustment in the Pd potential can be viewed as a means of incorporating the host and impurity interactions (i.e., the effects of charge rearrangement upon alloying) which represent an important physical effect in the alloy.

In considering the theoretical spectrum of Cu-rich CuPd alloys, Figs. 1 and 2 show that the Cu  $d$ -band complex remains well defined in the alloy. The dominant effect of Pd is to cause the appearance of two broad impurity bands centered around 1.7 and 5.0 eV below  $E_F$ , lying, respectively, above and below the Cu  $d$  bands.<sup>17</sup> The reason that these bands are depicted simply as hatched regions of roughly the full width at half maximum of the associated structures in the Pd density of states [e.g., the structures  $A_{Pd}$  and  $B_{Pd}$  in Fig. 1(d)] is that in view of their large disorder smearing, the crystal momentum  $\vec{k}$  for these states is not well conserved, and a complex band calculation is not very useful in this case. (In fact, for similar reasons, the other Pd derived  $d$  bands are also not shown explicitly in these figures.) The splitting between the two aforementioned Pd  $d$  bands physically has its origin in the effect of the (cubic) crystal field, a point we will elaborate upon shortly. With increasing Pd concentration, as the Pd  $d$  bands begin to develop, the density of states between the peaks tends to increase. This effect can be seen clearly by comparing Figs. 1(d) and 2(d), which show the Pd component density states in 5 and 15 at. % Pd, normalized to the same value and also in Figs. 3(a) and 3(b). Finally, we note that, in contrast to the  $d$ -like part of the spectrum which undergoes large changes, the  $s$ - $p$  states

of Cu are not influenced as much by Pd; for example,  $\Gamma_1$ ,  $X_4$ , and  $L_{2'}$  levels suffer shifts of only a few tenths of an electron volt in  $Cu_{85}Pd_{15}$ .

The spectrum of CuPd alloys thus differs strikingly from that of other Cu-based solid solutions such as CuNi, CuZn, CuAl, and CuGe. As discussed elsewhere,<sup>2</sup> in CuAl and CuGe, the disorder is large for states of  $s$ - $p$  symmetry and relatively small for the  $d$ -like states. In CuNi and CuZn, on the other hand, the situation is reversed in that most of the disorder is confined to the  $d$  channel. However, Ni in CuNi (or Pd in AgPd) induces only a single impurity band lying above the host  $d$  bands,<sup>12-14</sup> whereas Pd in CuPd yields two well-resolved impurity bands. Figure 4 offers further insight into these phenomena. Figure 4(a) compares the  $\Gamma$  to  $X$  energy bands in hypothetical pure crystals corresponding to the Pd and Cu muffin-tin potentials used in the CuPd alloy computations. A similar plot of Cu and Ni bands appropriate for the CuNi system is given in Fig. 4(b). All the bands in CuNi are seen to be clearly split [Fig. 4(b)], whereas the situation is seen to be more complicated in CuPd. The  $\Delta_2$  and  $\Delta_2'$  bands of Cu and Pd in Fig. 4(a) are quite distinct but the  $\Delta_5$  and  $\Delta_1$  bands cross each other. Recall that in a fcc lattice, the crystal-field-split atomic states of  $e_g(\Gamma_{12})$  and  $t_{2g}(\Gamma_{25'})$  symmetry are spread over the entire  $d$  band (see, for example, Fig. 2 of Ref. 18). The presence of the Cu  $d$  band in the middle of the broad Pd  $d$  band then tends to repel the  $e_g$ -type states in the lower part of the Pd  $d$  band into the lower density of states peak B [Fig. 1(d)] and similarly, the  $t_{2g}$ -type states lying in the upper portion of the Pd  $d$  band into the upper impurity peak A. Thus, not only does the peak A (or B) consist of split-band contributions of  $e_g$  (or  $t_{2g}$ ) type, but it also develops an admixture of  $t_{2g}$  (or  $e_g$ ) symmetry, even for very low Pd concentrations. It should be obvious that these effects will occur more generally whenever the host possesses a narrow  $d$  band, the impurity a broad band, and when the

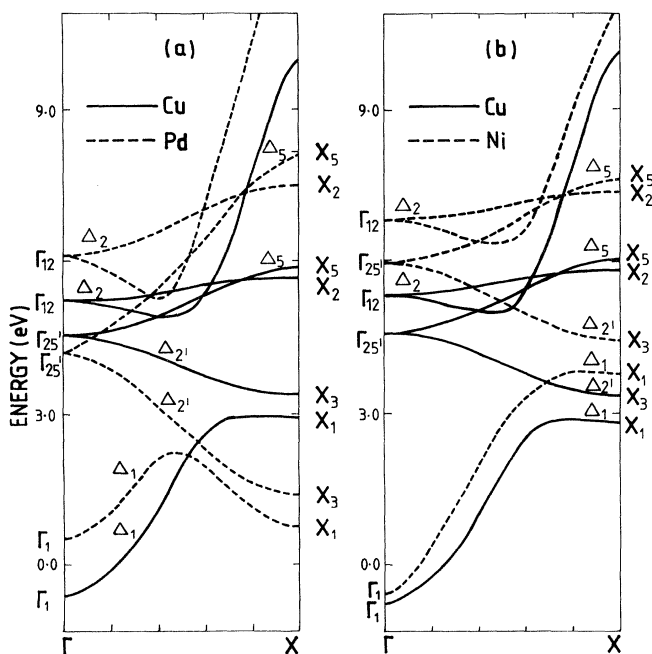


FIG. 4. (a)  $\Gamma$ - $X$  energy bands if the Cu and Pd potentials used in the present CuPd computations are placed on the fcc Cu lattice. (b) Same as (a) except that this figure refers to the Cu and Ni bands relevant in CuNi alloys.

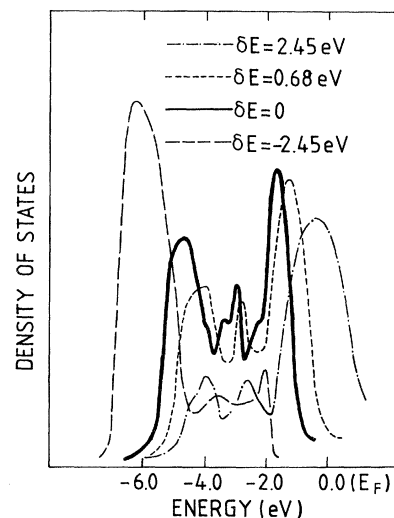


FIG. 5. KKR-CPA densities of states on Pd site in  $Cu_{85}Pd_{15}$  for a number of shifts  $\delta E$  of the Pd muffin-tin potential with respect to the Cu potential.  $\delta E = 0$  corresponds to the correct Pd potential in the alloy.

former lies approximately in the middle of the latter. The aforementioned reasons of symmetry are also behind the fact that the uppermost valence band (i.e., the band which terminates at  $X'_4$  or  $L'_2$ ), hybridizes strongly with the upper Pd-impurity band as it crosses the latter along the  $\Gamma-X$  symmetry direction in Figs. 1(a) and 2(a) (indicated by a break in this band in the figure). By contrast, along the  $\Gamma-L$  direction, there is no hybridization, although the presence of an admixture of states of  $t_{2g}$ -type symmetry in the upper impurity band does cause an increased smearing as the two bands cross [Figs. 1(b) and 2(b)].

We have also carried out a number of additional KKR-CPA calculations in  $\text{Cu}_{85}\text{Pd}_{15}$  and  $\text{Cu}_{95}\text{Pd}_5$  in which the Pd muffin-tin potential was shifted by a constant amount  $\delta E$  from its correct value. In this connection, Fig. 5 shows the component density of states on a Pd site for positive as well as negative values of  $\delta E$ , the  $\delta E=0$  curve (solid) being the same as that plotted in Fig. 2(d). For the positive shift  $\delta E=2.45$  eV, both the  $\Gamma_{12}$  and  $\Gamma_{25'}$  Pd levels move above the Cu  $d$  bands, and only a single dominant impurity peak at about  $-0.4$  eV (chain curve) is obtained. As  $\delta E$  decreases to 0.68 eV, the structure in the low-energy region around  $-4.2$  eV begins to develop (short-dashed curve) and it is fully developed for  $\delta E=0$ . Finally, for  $\delta E=-2.45$  eV, both  $\Gamma_{12}^{\text{Pd}}$  and  $\Gamma_{25'}^{\text{Pd}}$  pass below the Cu  $d$  bands, and once again a single pronounced structure (at low energy) is obtained. It is noteworthy that, as  $\delta E$  decreases from 2.45 to 0.0 eV, the impurity peak around  $-1.7$  eV gets reduced in weight, becomes narrower and, in fact, its inner edge at approximately  $-2.1$  eV appears to become sharper,<sup>19</sup> presumably due to the aforementioned repulsion of the Pd  $d$  states which becomes stronger as the Pd  $d$  bands approach the Cu  $d$  bands.

We conclude this section by pointing out that the large effective crystal-field splitting on the Pd sites in  $\text{CuPd}$  results from a combination of two effects. (i) The lattice constant of Cu (6.831 a.u.) and also of  $\text{CuPd}$  (6.862 a.u. in 5 at. % Pd and 6.923 a.u. for 15 at. % Pd) is substantially smaller than the Pd crystal (7.353 a.u.). The Pd potential, generated on the smaller  $\text{CuPd}$  lattice, possesses a larger crystal-field splitting compared to a pure Pd crystal. (ii) As already noted, the  $\Gamma_{12}^{\text{Pd}}$  and  $\Gamma_{25'}^{\text{Pd}}$  levels of Pd lie, respectively, above and below the corresponding Cu levels, and alloying further splits them apart due to the repulsion from Cu levels. Consequently, a splitting of 1.4 eV between the  $\Gamma_{12}$  and  $\Gamma_{25'}$  levels in a pure Pd crystal is increased to a separation of approximately 3.0 eV in  $\text{CuPd}$ , as deduced from the positions of the peaks  $A_{\text{Pd}}$  and  $B_{\text{Pd}}$  in Fig. 1(d). By contrast, in Cu-Ni the host and impurity lattice constants are quite close to each other, and in  $\text{AgPd}$  the lattice constant is larger than that in Pd, causing this splitting to be reduced.

### III. ANGLE-RESOLVED PHOTOEMISSION MEASUREMENTS AND COMPARISON BETWEEN THEORY AND EXPERIMENT

The angle-resolved photoemission measurements were performed using a multitechnique photoelectron spectrometer operated at an energy resolution of 100 meV. The NeI (16.85 eV) and HeI (21.22 eV) resonance lines

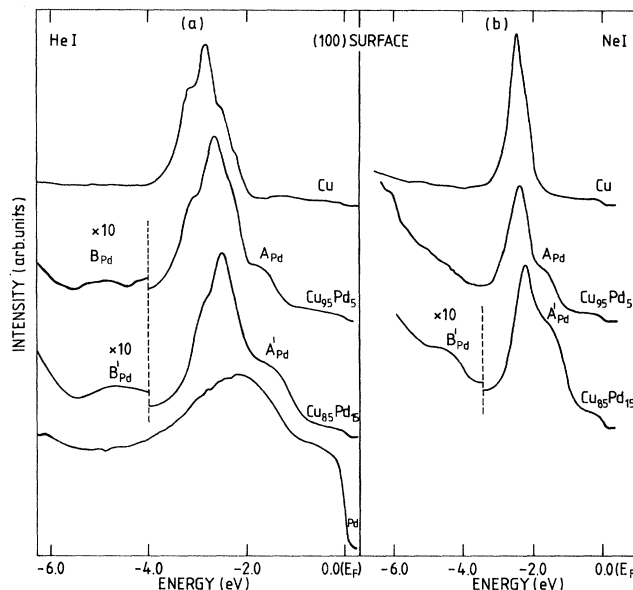


FIG. 6. HeI and NeI angle-resolved normal emission spectra from the (100) face of Cu,  $\text{Cu}_{95}\text{Pd}_5$ ,  $\text{Cu}_{85}\text{Pd}_{15}$ , and Pd. The Pd- and Cu-derived structures, identified by various letters, are discussed in the text. The spectra for energies below the vertical broken lines are drawn on an expanded scale to show the Pd-related structures  $B_{\text{Pd}}$  and  $B'_{\text{Pd}}$  clearly.

produced from a gas-discharge lamp were used to induce electron emission. The  $\text{CuPd}$  crystals were grown by the Bridgman method. They were cut along the low-index planes (100), (110), and (111) to an accuracy of  $\pm 1^\circ$ . The crystals were polished mechanically and electrochemically and cleaned under ultrahigh vacuum conditions in the

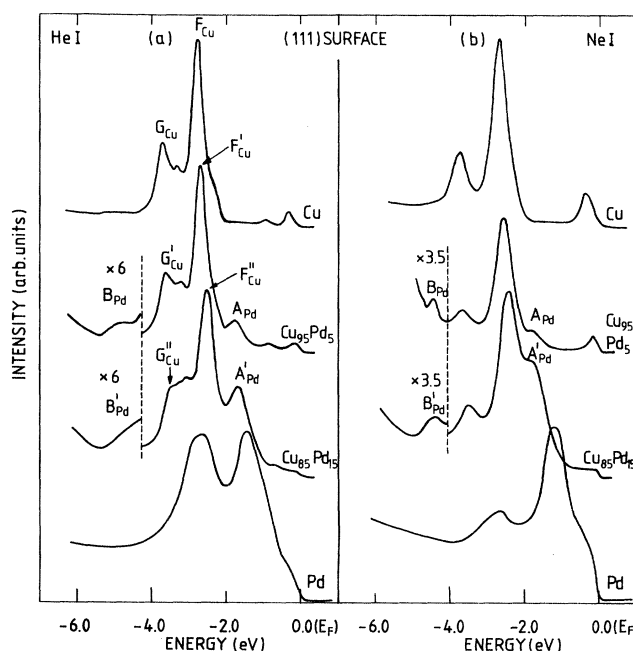


FIG. 7. Same as the caption to Fig. 6, except that this figure refers to the (111) surface.

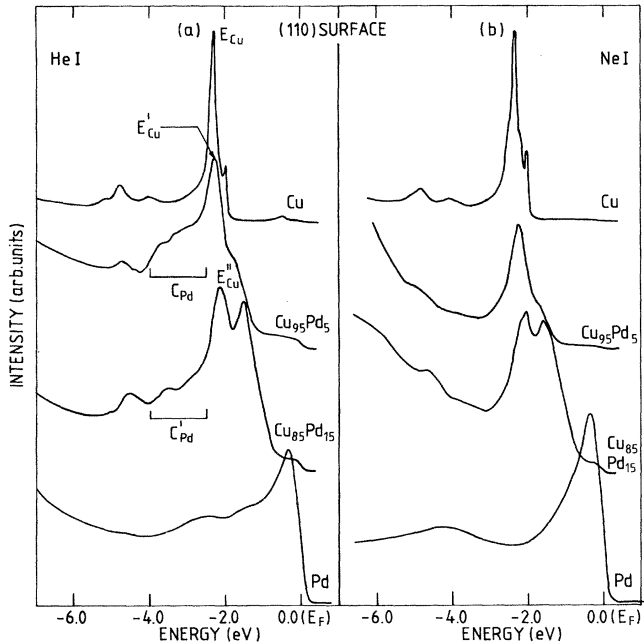


FIG. 8. Same as the caption to Fig. 6 except that this figure refers to the (110) surface.

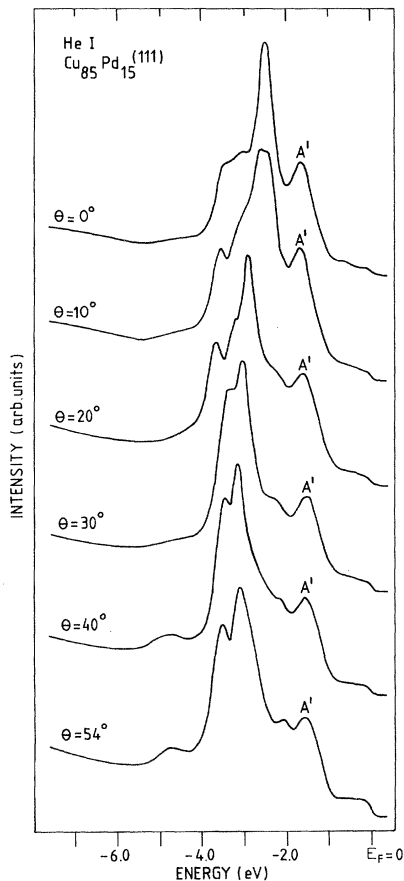


FIG. 9. Off-normal He I angle-resolved photoemission spectra from  $\text{Cu}_{85}\text{Pd}_{15}(111)$  for various polar angles  $\theta$ . The Pd peak  $A'$  is identified.

spectrometer by annealing at 720 K for 30 min and bombarding with  $\text{Ar}^+$  ion for a few minutes at 1 keV. The cleaning procedure was repeated several times until no surface contaminants were observed in Auger-electron spectroscopic measurements. The surface composition was found to be the same as that of the bulk solid for the (100) and (111) faces. A slight Pd enrichment could be detected for the (110) surface. Low-energy electron diffraction (LEED) patterns exhibited sharp spots with the normal  $(1 \times 1)$  surface structure for all the samples studied.

We discuss now how the theoretical picture developed in Sec. II above compares with the angle-resolved photoemission measurements from the low-index faces of Cu,  $\text{Cu}_{95}\text{Pd}_5$ ,  $\text{Cu}_{85}\text{Pd}_{15}$ , and Pd single crystals. The normal emission spectra of Figs. 6–9 reveal that the Cu  $d$ -band complex continues to be clearly identifiable in the alloy and that the addition of Pd induces new states in the energy range of 1–2 eV and also from about 4 to 5.8 eV below  $E_F$ . Off-normal-emission measurements (see Fig. 9) show that the two aforementioned structures possess only a slight dispersion, even in the 15-at. % Pd alloy, and thus the associated states are widely spread out in  $\vec{k}$  space, in accord with the calculations.<sup>20</sup> The Pd states between the main impurity peaks  $A_{\text{Pd}}$  and  $B_{\text{Pd}}$  shown in Fig. 1(d) are exhibited clearly in the experimental spectra for 21.22-eV emission from the (110) surface. These structures labeled  $C_{\text{Pd}}$  and  $C'_{\text{Pd}}$  in Fig. 8(a) are difficult to discern in other spectra because they will presumably be masked by the strong emission from Cu states, which are absent only in this special case; an increased intensity upon alloying between the Cu peaks  $G_{\text{Cu}}$  and  $F_{\text{Cu}}$  can, however, be seen in the He I (111) spectra in Fig. 7(a). The  $E$ - $\vec{k}$  positions of the various Cu peaks in Cu,  $\text{Cu}_{95}\text{Pd}_5$ , and  $\text{Cu}_{85}\text{Pd}_{15}$  are

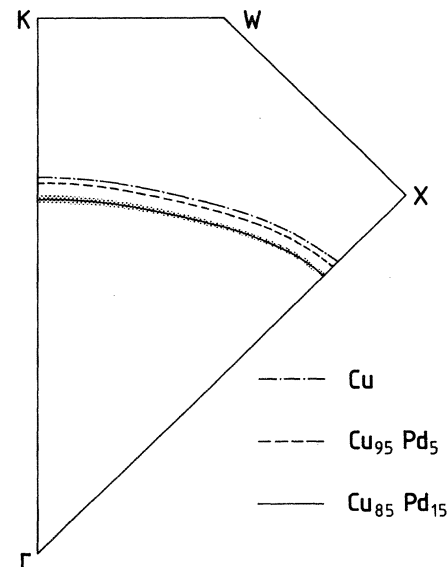


FIG. 10. Calculated cross sections of the Fermi surfaces of Cu,  $\text{Cu}_{95}\text{Pd}_5$ , and  $\text{Cu}_{85}\text{Pd}_{15}$  with the (100) plane  $\Gamma X W K \Gamma$  in the Brillouin zone. The length of the shading around the alloy curves gives the magnitude of the smearing  $2|\Delta\vec{k}(E_F)|$  of the Fermi surface in momentum space.

determined straightforwardly from the experimental data using the triangulation (energy coincidence) method of photoemission<sup>21</sup> and are indicated by crosses in Figs. 1 and 2. The estimated full width at half maximum of the Pd structures  $A_{Pd}, B_{Pd}, C_{Pd}$  and  $A'_{Pd}, B'_{Pd}, C'_{Pd}$  read from the spectra is shown by cross-hatched markings on the right side of the  $\Gamma-X$ ,  $\Gamma-L$ , and  $U-X$  panels. Agreement between the computations and measurements with respect to the absolute positions of the Cu-derived levels in both the 5- and 15-at. % alloy as well as the energies and characteristic widths of the two Pd-derived impurity bands is seen to be remarkably good; discrepancies especially with respect to the width of the lower structure (peak  $B_{Pd}$ ) are not significant since this quantity is difficult to read precisely from the spectra.

The width of the two Pd-induced impurity bands in the 5-at. % alloy represents primarily the disorder smearing of these states. Of course, as the Pd concentration increases, some of the observed width is associated with the emergence of the Pd  $d$  bands. Our experiments also provide information about the damping of the Cu-derived states in the alloy. For example, the peak  $E_{Cu}$  in Fig. 8(a) is seen to broaden rapidly on alloying; the estimated increase in the full width in  $Cu_{85}Pd_{15}$  is 0.60 eV, fully consistent with

the corresponding calculated value of 0.49 eV. The peak  $F_{Cu}$  in Fig. 7(a) suffers less smearing than  $E_{Cu}$ . This can be understood by noting that the  $\bar{k}$  value for the peak  $E_{Cu}$  lies near the top of the Cu  $d$  band around the symmetry point  $X$  [Figs. 1(c) and 2(c)], while that for the peak  $F_{Cu}$  lies quite close to the center of the zone [Figs. 1(b) and 2(b)]. Therefore, the relative broadening of the peaks  $E_{Cu}$  and  $F_{Cu}$  confirms the calculated  $k$  dependence of the width of the uppermost Cu  $d$  band, which increases for increasing  $k$  values [Fig. 2(b)]. Finally, it is noteworthy that the peak  $G_{Cu}$  is virtually undamped as may be deduced from the similarities of the low-energy side of this peak for pure Cu and  $CuPd$ ; see Fig. 7(a). Our calculations show, indeed, that the lower part of the Cu  $d$ -band complex giving rise to the peak  $G_{Cu}$  is much less damped than the upper part of the  $d$ -band regime. A similar good level of agreement is found for a variety of other spectral features.

Figure 10 considers the changes in the cross section of the Cu Fermi surface (FS) in the  $\Gamma XWK\Gamma$  plane. The computed decreases in the volumes of the two alloy FS's are approximately proportional to the Pd concentration, as would be predicted by a rigid-band model assuming a valence of zero for Pd and one for Cu. In the Cu-rich re-

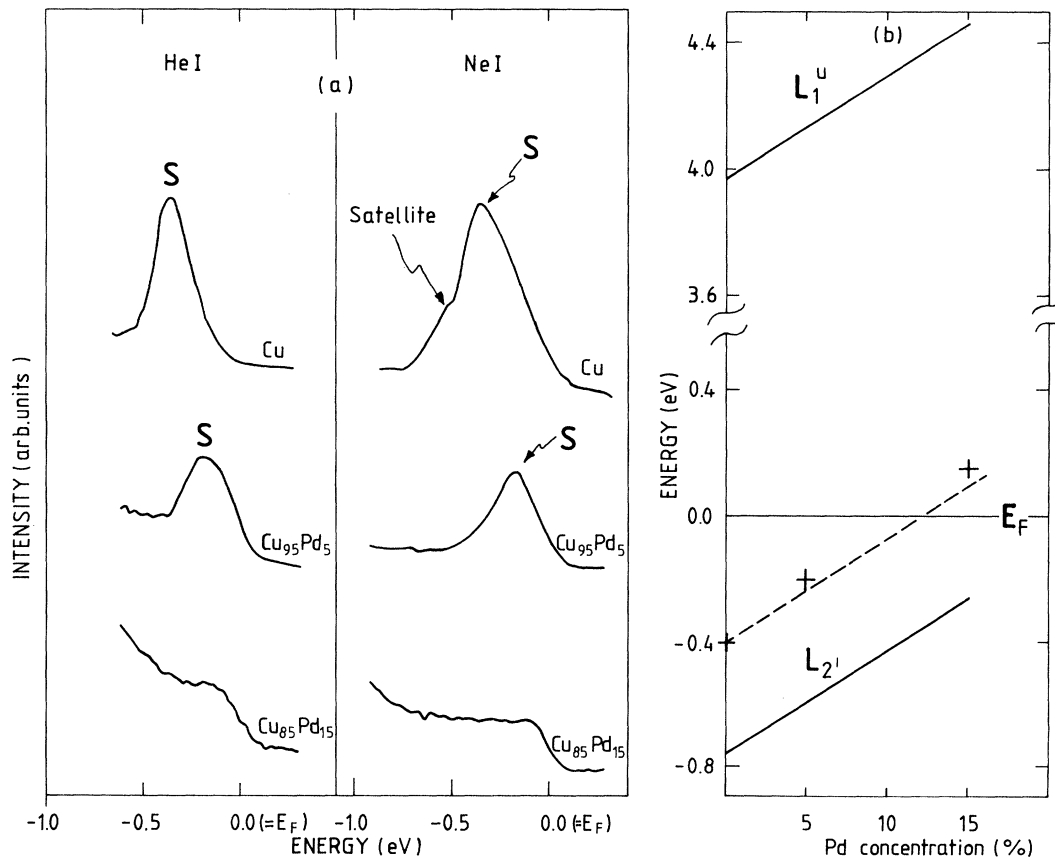


FIG. 11. (a) He I and Ne I spectra of Fig. 7 for the (111) surface are shown on an expanded scale in the energy region of the  $\Gamma$  centered (111) Shockley state. (b) Positions of the  $L_{2'}$  and  $L_1^u$  levels with respect to the Fermi energy  $E_F$  are plotted as a function of the Pd concentration. Note the break in the scale for the  $L_1^u$  curve. Crosses indicate the experimental positions of the (111) Shockley states in Cu,  $Cu_{95}Pd_5$ , and  $Cu_{85}Pd_{15}$  (Refs. 24). The dashed line, drawn parallel to the  $L_{2'}$  curve through the Cu data point, represents the theoretically estimated position of the surface state in the alloy.

gime this is to be anticipated since, as noted above, the uppermost  $s$ - $p$  band (responsible for the FS) is not affected much on alloying; this is also the case on other Cu-based solid solutions such as  $CuZn$ . (Of course, for large enough Pd content the Pd  $d$  bands will intersect the Fermi energy and cause strong deviations from a Cu-like FS.) Finally, we point out that the disorder-induced full width at half maximum,  $2|\Delta\vec{k}|$ , of the FS dimensions increases from 0.05 to 0.1 mrad in going from the  $\Gamma$ - $X$  to the  $\Gamma$ - $K$  direction in  $Cu_{85}Pd_{15}$ . This is the result of an increased  $d$  admixture in the associated states at the  $E_F$ . As emphasized elsewhere,<sup>22</sup> the  $\vec{k}$  width  $2|\Delta\vec{k}|$  should be distinguished from the corresponding width in energy, shown by shading around the levels in Figs. 1 and 2.

The behavior of the Shockley as well as the Tamm-type intrinsic surface states on the low-index faces of Cu and  $CuAl$  was discussed at some length in Ref. 7. In  $CuPd$ , in Fig. 11 (and also Fig. 7) shows that the (111) Shockley state moves from a binding energy of 0.4 eV in Cu to about 0.2 eV in  $Cu_{95}Pd_5$ . For 15-at. % Pd the enhanced intensity observed near the  $E_F$  indicates that this state has moved just above the Fermi energy.<sup>23</sup> The Tamm states which lie very close to the Cu  $d$ -band edge on the Cu(100) and (111) surfaces are not expected to be observable in the  $CuPd$  spectra, since Pd yields a strong emission in the same energy range. Recall that the (111) Shockley state is tied to the bulk energy gap between the  $L_{2'}$  and  $L_1^u$  levels and is characterized by an  $s$ - $p$  type symmetry. Therefore, variations in the bulk  $L_{2'}$  and  $L_1^u$  levels can be used to

monitor this state in the alloy. The computed position of the  $L_{2'}$  and  $L_1^u$  levels are displayed in Fig. 11(b). In the present case, both these levels move in essentially the same manner. The parallel dashed line drawn through the Cu data point then yields the estimated position of the Shockley state in the alloy. It is gratifying that the experimental values in both the 5- and 15-at. % alloys are quite close to the theoretical predictions.<sup>24</sup> The surface state is predicted to cross the  $E_F$  at approximately 12-at. % Pd. The disorder smearing of the  $L_{2'}$  and  $L_1^u$  levels is also reflected in the increased broadening of the (111) Shockley state peak  $S$  in the alloy. The full widths at half maxima of the peak  $S$  in the He I spectra of Fig. 11(a) are estimated to be 180 and 240 meV in Cu and  $Cu_{95}Pd_5$ , respectively. (The Ne I spectra are not useful for this purpose, since they contain a closely placed satellite structure below the peak  $S$ , visible clearly in the Cu curve.) The preceding increase of 60 meV (Refs. 25 and 26) compares well with the corresponding calculated value of 45 meV for the average disorder smearing of the  $L_{2'}$  and  $L_1^u$  levels in the 5-at. % Pd alloy.

#### ACKNOWLEDGMENTS

We would like to acknowledge important conversations with Dr. R. Prasad and the technical assistance of Mr. A. Vuoristo. This work was supported in part by the U.S. National Science Foundation and by the Finnish Academy of Sciences (Contract Nos. 15/26/1980 and 61/1981).

<sup>1</sup>For a recent theoretical review and further literature citations on alloys, see Refs. 2 and 3.

<sup>2</sup>A. Bansil, in *Positron Annihilation*, edited by P. G. Coleman, S. C. Sharma, and L. M. Diana (North-Holland, Amsterdam, 1982), p. 291.

<sup>3</sup>J. S. Faulkner, in *Progress in Material Science*, edited by T. Massalski (Pergamon, New York, 1982), Vol. 27.

<sup>4</sup>For a recent review of work on alloys, see A. Bansil and M. Pessa, *Phys. Scr.* **74**, 52 (1983).

<sup>5</sup>S. Berko, in *Positron Annihilation*, edited by R. R. Hasiguti and K. Fujiwara (Japan Institute of Metals, Sendai, 1979).

<sup>6</sup>R. E. Hummel, *Phys. Status Solidi A* (in press).

<sup>7</sup>H. Asonen, M. Lindroos, M. Pessa, R. Prasad, R. S. Rao, and A. Bansil, *Phys. Rev. B* **25**, 7075 (1982).

<sup>8</sup>A. Bansil, R. S. Rao, R. Prasad, H. Asonen, and M. Pessa, *J. Phys. F* (in press).

<sup>9</sup>N. Martensson, R. Nyholm, H. Calén, J. Hedman, and B. Johansson, *Phys. Rev. B* **24**, 1725 (1981).

<sup>10</sup>P. Weightman, P. T. Andrews, G. M. Stocks, and H. Winter, *J. Phys. C* **16**, L81 (1983). These authors analyze the Auger spectra of Cu-Pd and Ag-Pd alloys in the light of their KKR-CPA calculations and conclude that the Pd impurity spectra in  $CuPd$  is substantially broader than in  $AgPd$ .

<sup>11</sup>L. E. Walldén, *Solid State Commun.* **7**, 593 (1969).

<sup>12</sup>A. Bansil, *Phys. Rev. B* **20**, 4025 (1979); **20**, 4035 (1979).

<sup>13</sup>B. E. A. Gordon, W. E. Temmerman, and B. L. Gyorffy, *J. Phys. F* **11**, 821 (1981).

<sup>14</sup>A. J. Pindor, W. M. Temmerman, B. L. Gyorffy, and G. M.

Stocks, *J. Phys. F* **10**, 2617 (1980).

<sup>15</sup>F. M. Mueller, A. J. Freeman, J. O. Dimmock, and A. M. Furdyna, *Phys. Rev. B* **1**, 4617 (1970).

<sup>16</sup>M. Pessa and O. Jylhä, *Solid State Commun.* **46**, 419 (1983).

<sup>17</sup>Of course, there are other smaller structures associated with the Pd  $d$  bands, as is evident from Figs. 1(d) and 2(d). We emphasize further that the Cu and Pd  $l=2$  phase shifts cross at about 3.0 eV below  $E_F$  in both  $Cu_{95}Pd_5$  and  $Cu_{85}Pd_{15}$ . Therefore, the effective disorder in the alloy will be quite small around this energy, and the Pd states will experience little effects of disorder, even though the Pd states in general are heavily damped. Interestingly, Figs. 1(d) and 2(d) show the presence of a peak in the density of states around 3.0 eV below  $E_F$ .

<sup>18</sup>G. M. Stocks, R. W. Williams, and J. S. Faulkner, *Phys. Rev. B* **4**, 4390 (1971).

<sup>19</sup>This effect is seen more clearly in the 5-at. % Pd computations (not shown).

<sup>20</sup>The slight dispersion of the upper impurity band (i.e., the band  $A'_{Pd}$  in Fig. 2) is difficult to calculate theoretically due to the large disorder smearing. However, our calculations in  $Cu_{75}Pd_{25}$  show that the computed  $\vec{k}$  dependence is consistent with that deduced from Fig. 9 for the peak  $A'_{Pd}$ .

<sup>21</sup>See, for example, M. Pessa, M. Lindroos, H. Asonen, and N. V. Smith, *Phys. Rev. B* **25**, 738 (1982).

<sup>22</sup>R. Prasad, S. C. Papadopoulos, and A. Bansil, *Phys. Rev. B* **23**, 2607 (1981).

<sup>23</sup>Although we have not carried out the necessary off-normal-

emission measurements, the (110) Shockley state in  $CuPd$  will presumably behave in a manner similar to the (111) Shockley state.

<sup>24</sup>In 15-at. % Pd spectra, the experimental surface state must obviously lie above but (about) within the width of the peak in order to give a substantial enhancement of intensity below the Fermi energy. This fact was used to estimate the position of the peak.

<sup>25</sup>Additional broadening mechanisms of this Shockley state, as explained in Ref. 26, do not contribute to this value because the position of the surface state with respect to the bulk continuum in  $Cu_{95}Pd_5$  remains the same as that in Cu, and the peak widths are compared for normal emission from (111) surfaces.

<sup>26</sup>S. D. Kevan, Phys. Rev. Lett. 50, 526 (1983).